UNIVERSITY HONORS PROGRAM

SENIOR PROJECT - APPROVAL

Name: Erin M. McMahon

College: Arts & Sciences Department: Physics and Astronomy

Faculty Mentor: Dr. Mike Guidry

PROJECT TITLE: A Stochastic Algorithm for Element Production in Stars

I have reviewed this completed senior honors thesis with this student and certify that it is a project commensurate with honors level undergraduate research in this field.

Signed: M W Guidry, Faculty Mentor

Date: 05/03/02

Comments (Optional):

A Stochastic Algorithm for Element Production in Stars

Erin McMahon
Dr. Mike Guidry
University of Tennessee Department of Physics and Astronomy

Introduction

Since the beginning of the 20th century, we have known that stars generate energy to balance their gravitational contraction through nuclear reactions. Deep in the core, the process of hydrogen burning begins the manufacturing of elements and isotopes that we can observe from telescopes on earth and on satellites. Observed elemental and isotopic signatures characterize the nucleosynthesis processes that occur during the evolution and death of a star. These observations better enable us to model the mechanisms occurring in this environment.

Currently, the method used for simulating stellar nuclear processes involves solving sets of coupled ordinary differential equations based on the rates of production and depletion of elements and isotopes. In this paper, we will concentrate on a new algorithm for this type of calculation, more specifically, a stochastic algorithm. In the first section, a brief summary of the nuclear processes in stellar astrophysics will be given. Results from this algorithm are to be compared to those coming from the current thermonuclear reaction network in two test cases: the CNO cycle and the hot CNO cycle, both at constant temperature and density.

Hydrostatic and Explosive Burning Stages

2.1. Hydrostatic Burning Stages and Stellar Evolution

A star's life is comprised of a series of burning stages. The burning of a new type of nuclear fuel characterizes each stage. A star with the mass of the sun will burn both hydrogen and helium, while more massive stars (those with masses of roughly 8 times that of the sun) burn isotopes through silicon. As the star consumes each type of nuclear fuel, the compression from gravity creates the higher temperatures and densities necessary to overcome the increasing Coulomb repulsion of the more massive reactants in the subsequent stage.

Hydrostatic burning stages begin in the core of the star. The final burning stage of a each star depends most critically on its mass. As you can see in the HR-diagram (Hertzsprung-Russell diagram) on the left, most stars near our sun are in the main sequence, the s-shaped band near the center. The more massive stars pass quickly through this region and become giants and supergiants, while the smaller stars only move partially through the region, eventually becoming white dwarfs. More massive and brighter stars evolve more quickly, staying on the main sequence on the order of a million years. Smaller stars remain here for several hundred billion years.

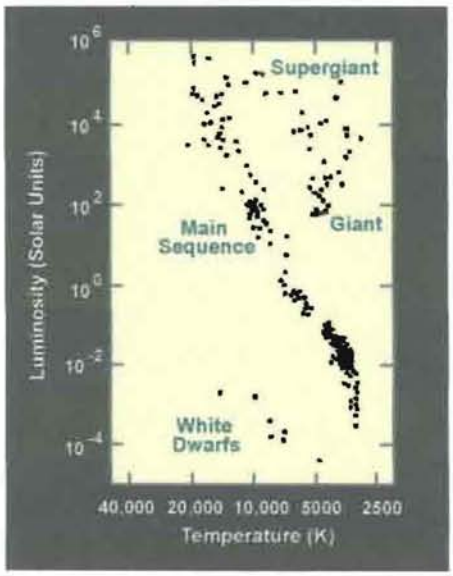

Figure 1: HR diagram for stars near our sun.

Stars spend most of their lifetime in the main sequence. Here, the star proceeds through the hydrogen core burning stage.

The stability of a star depends on the balance between the pressure trying to expand the star (heat of fusion during fuel burning) and the gravitational force trying to contract it (see **Figure 2**). This is called hydrostatic equilibrium; thus the burning stages that occur during this time are normally called hydrostatic burning stages. Since timescales for beta-decays are short compared to hydrostatic burning timescales, nuclei have a chance to decay back to stable isotopes before undergoing a different reaction. Thus, hydrostatic burning stages, for the most part, are limited to stable isotopes.

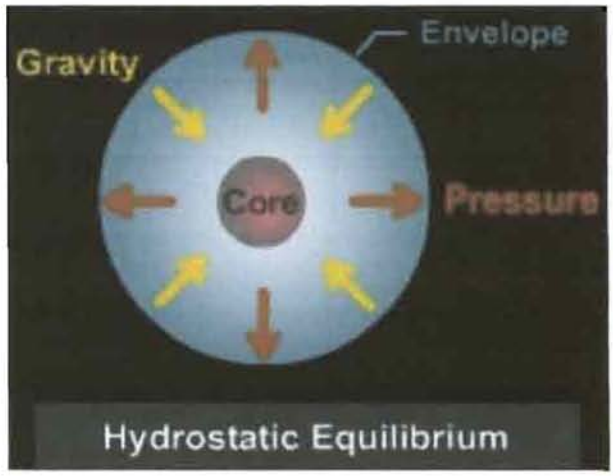

Figure 2: Hydrostatic equilibrium in a star. Pressure from thermonuclear reactions in the core balances the gravitational pressure pressing inward.

The lighter stars only burn fuel through helium, since the packing of the electrons into a degenerate Fermi-Dirac configuration provides sufficient pressure to support the star against further gravitational contraction. The remaining envelope of these smaller stars is blown off, forming a planetary nebula, leaving the core behind, the white dwarf. The larger stars that progress further through burning stages cannot support the gravitational contraction during the last burning stage (silicon burning); the growing iron core cannot undergo any fusion reactions, so the gravitational squeeze quickly becomes gravitational collapse. The end result is a Type II core collapse supernova, finally resulting in either a neutron star or a black hole.

The hydrogen burning stage takes place under low temperatures (compared to explosive temperatures) ranging from .02 to .05 GK (GK=10^9 Kelvin). In those stars whose mass is equal to or less than the sun, this takes place via the proton-proton (P-P) chain. **Figure 3** explains how the proton-proton chain occurs.

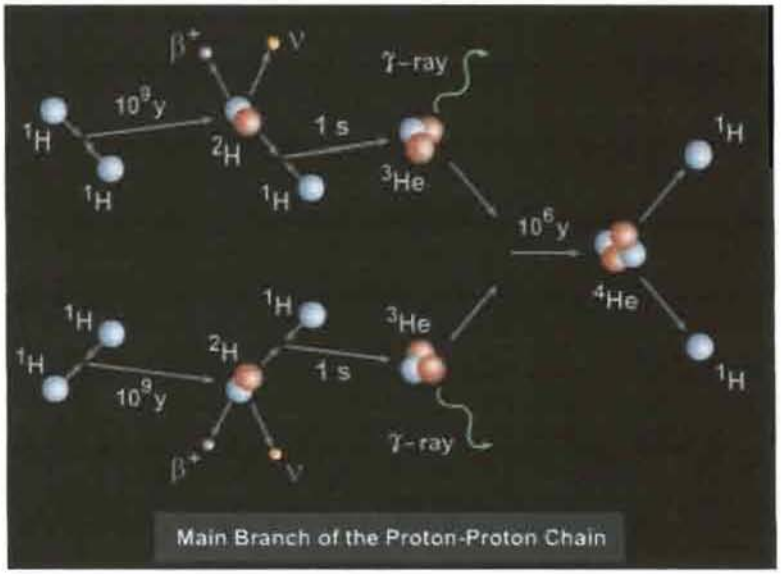

Figure 3: The proton-proton chain.

For stars with masses that are greater than that of the sun, hydrogen burning mainly proceeds by the CNO (carbon, nitrogen, and oxygen) cycle. The small amounts of carbon, nitrogen, and oxygen isotopes are catalysts; these elements are not produced in large amounts at this time. A small amount of each of these pre-existing isotopes is present in a bath of protons, making the proton capture reactions that are essential to the cycle possible.

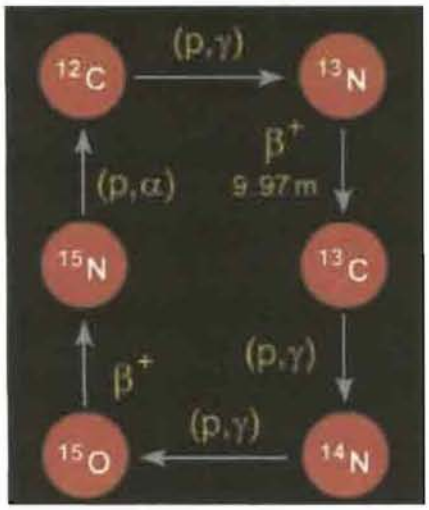

Figure 4: The CNO cycle.

Through a series of (p,γ) reactions, beta-decays, and a (p,α) reaction, alpha particles or ^{4}He are produced (see **Figure 4**). The "ashes" of hydrogen burning are mostly helium, which now makes up the new core.

At this point, life in the main sequence (core hydrogen burning sequence) is finished. The least massive stars proceed directly to white dwarf stage,

which is the end of their life. Stars with medium mass move to the red giant stages, where more fuel burning with higher mass isotopes takes place. The most massive stars also continue in advanced burning stages, becoming giants and supergiants.

Before the helium core starts its burning process in medium and large mass stars, the shell of hydrogen around the core continues burning. As a result of core contraction due to gravitational pressure in the red giant stage, the core then ignites, producing carbon through the triple-alpha process (see **Figure 5**, right). In more massive stars, some ^{12}C captures another α-particle to form ^{16}O. This burning occurs at a temperature of about 0.05 to 0.3 GK. This is sometimes called the Helium Main Sequence, but it is much shorter than the [hydrogen] Main Sequence. Stars in the red giant phase are now finished burning fuel. They will now undergo surface mass loss and ejection of planetary nebula, then moving to the white dwarf stage as well. The most massive stars, however, still continue to consume fuel via shell and core burning.

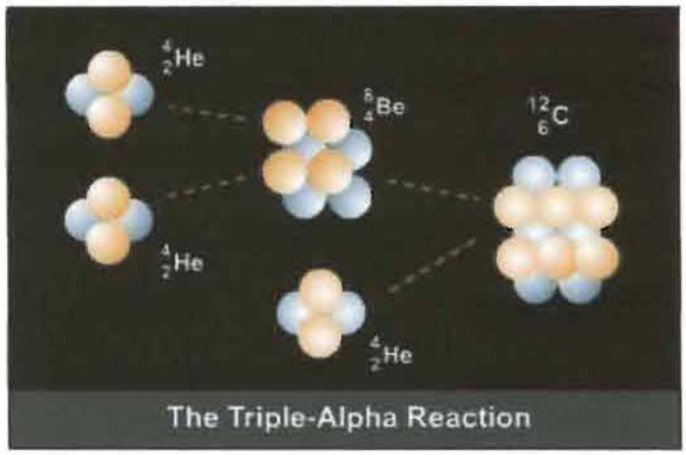

Figure 3: The triple-alpha process for helium burning.

Carbon burning is the first advanced burning stage. Stars entering this phase are typically more massive than 4 $M_\odot$ (solar masses), at a temperature of about 0.5 GK and density of about 3×10^6 g cm^{-3}. The reactions that take place include:

$$^{12}C + {}^{12}C \rightarrow {}^{20}Ne + \alpha \qquad ^{12}C + {}^{12}C \rightarrow {}^{23}Na + p \qquad ^{12}C + {}^{12}C \rightarrow {}^{23}Mg + p$$

The next stage is neon burning, which takes place at a temperature of ~3 GK. This stage and those following require a minimum mass of about 8 $M_\odot$. The two-step reaction proceeds as follows:

$$\gamma + {}^{20}\mathrm{Ne} \rightarrow {}^{16}\mathrm{O} + \alpha \qquad\qquad \alpha + {}^{20}\mathrm{Ne} \rightarrow {}^{24}\mathrm{Mg} + \gamma$$

As you can see, neon burning is initiated by a photodisintegration, freeing up an alpha particle for another ^{20}Ne to capture to form ^{24}Mg. Following neon burning, oxygen burns around a temperature of 2 GK by $^{16}\mathrm{O} + {}^{16}\mathrm{O} \rightarrow {}^{28}\mathrm{Si} + \alpha$. These ^{16}O particles exist from the photodisintegration of the ^{20}Ne particles in the first reaction in neon burning. All of these burning stages take place in core as well as shell burning.

Finally, silicon burning, at a temperature of about 3 GK, is the last burning stage, producing the rest of the elements up to the iron group. The first part of the process must be a photodisintegration (similar to the first neon reaction above), producing free alpha particles. Following the photodisintegration, the alpha particles then react with nuclei in reactions such as $\alpha + {}^{52}\mathrm{Fe} \leftrightarrow {}^{56}\mathrm{Ni} + \gamma$. Note here that temperatures are sufficient to also allow other photodisintegrations and charged particle captures, leaving many individual reactions in a chemical equilibrium where reactions are balanced by their inverse reactions [5]. This means that the effective rate at which silicon is burned is as much as 10^5 times slower than the individual reaction rates would indicate, since the reverse reactions occur almost as fast as their forward counterparts.

Members of the iron group are the last produced in hydrostatic burning. A star cannot produce energy by fusing nuclei beyond the iron region ($A \sim 60$) because that is where the peak of the binding energy curve (see **Figure 6**) is located. Those isotopes with $A < 60$ produce energy via fusion reactions, while those with $A > 60$ do so by fission

Figure 6: Curve of binding energy.

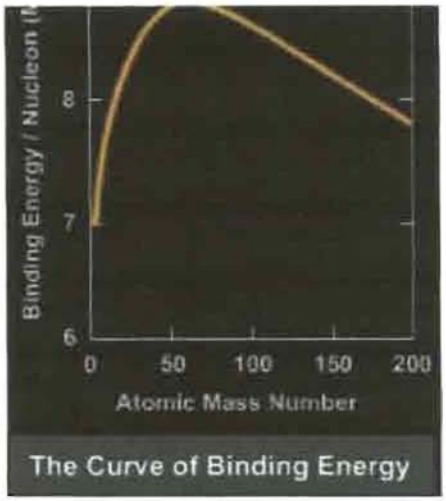

reactions of their own accord or forced fission reactions. The coulomb repulsion is also too great to fuse the isotopes with greater masses than that of oxygen. For larger atomic number, the nuclear charge increases and so does the Coulomb barrier of the charged particles. Thus, to fuse these particles heavier than oxygen, they need to be moving very fast. At higher temperatures, the heavy particles are able to be broken apart by photodisintegration, enabling these lighter particles to collide with the other heavy nuclei that have been broken apart as well.

During this last stage of burning, the balance of the star changes hands from hydrostatic burning pressure to electron degeneracy pressure in the core. The formation of the iron core marks the end of nuclear energy generation, because nuclei more massive than the iron peak nuclei are less bound. The core is stable initially, but since the shell source of silicon keeps producing a larger iron core, it

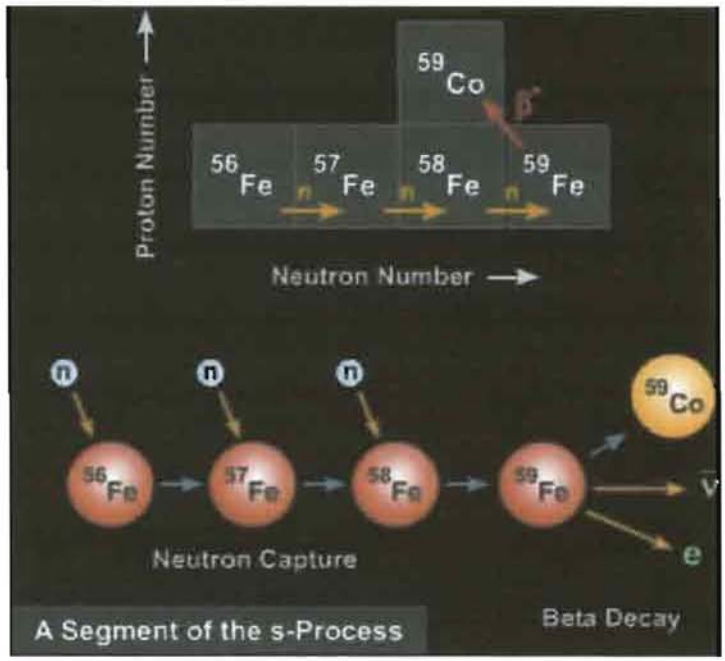

Figure 7: Some reactions of the s-process.

becomes unstable as it approaches the Chandrasekhar limit of about 1.44 $M_{\odot}$.

In addition to these burning stages, there also exists a process called the slow neutron capture process, or s-process (**Figure 7**). This process leads to the creation of the small abundances of approximately half of the heavy elements. Neutrons for this process are provided by (α,n) reactions in core and shell helium burning. An example of such a reaction is the $^{22}Ne(\alpha,n)^{26}Mg$ reaction. The free neutrons provided by such reactions initiate a series of neutron captures and beta-decays, starting with pre-existing medium and heavy nuclei up to iron, creating nuclei up to lead and bismuth. Temperatures for this process are in the range where photodisintegration reactions are not prominent [5].

2.2. Explosive Burning

Following the hydrostatic burning stages, explosive burning may occur. Explosions not only liberate nuclei trapped in the gravitational potential well of their parent star that were produced during hydrostatic burning stages, but also provide high temperature and density conditions for the production of many of the isotopes with masses between 16 and 70 (those that are heavier than 70 are also produced, via the r-process, discussed shortly). The initial hydrostatic composition of the star influences the ejected abundances from the explosively burned layers. The main fuels for explosive nucleosynthesis include ^{12}C, ^{16}O, ^{20}Ne, ^{24}Mg, and ^{28}Si [7].

For stars with mass greater than 8 $M_{\odot}$, an explosion can occur in the form of a core collapse supernova. This explosion begins when the gravitational pressure becomes too great for the iron core to withstand. This generally occurs when the mass of the iron core becomes larger than the Chandrasekhar mass. When the core reaches this mass, it

collapses, suddenly stopping when nuclear densities are reached in the material. Material falling toward the core bounces off this proto-neutron star, sending subsonic pressure waves outward from the center. After the subsonic pressure waves travel outward from the core, they finally pile up into a shockwave. This shockwave is formed when the speed of the pressure waves exceeds the speed of sound in the material. This shockwave begins to proceed through the layers composed of different nuclei formed during hydrostatic burning. The star before collapse resembles an onion; it has concentric layers of shell sources including the hydrogen, helium, etc. up to silicon, with an iron core at the center. These layers are enclosed by a mainly hydrogen envelope where no nuclear burning has occurred (**Figure 8**).

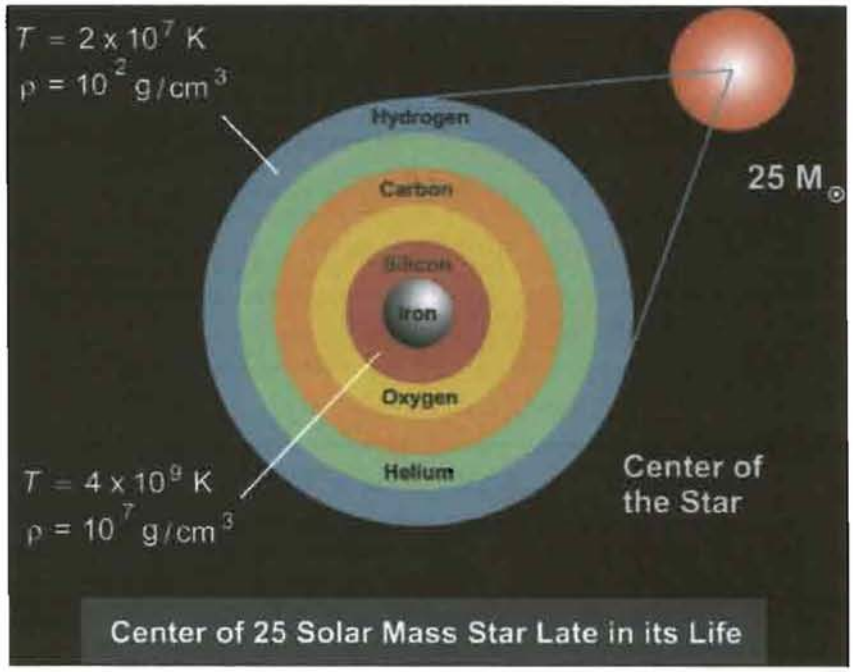

Figure 8: The spent fuel of the star forms concentric layers around a growing iron core.

Although the shockwave moving through this matter stalls, neutrinos moving outward from the center of the star reinvigorate the stalled shockwave, driving these layers into space, leaving behind a neutron star (if the core material was around 2-3 $M_\odot$) or a black hole. Energy released from this explosion is on the order of 10^{51} ergs, and the temperatures are around several

GK. Explosive burning occurs when this shockwave passes through the layers of material surrounding the core. Most of these reactions that occur here are those in that occur during hydrostatic burning stages, but with much shorter timescales (because of the higher temperatures and densities). The outer ejected layers do not undergo explosive nucleosynthesis. These layers give us insight into the hydrostatic burning stages in stellar evolution. The interior parts of the ejecta contain the information about the products of explosive burning.

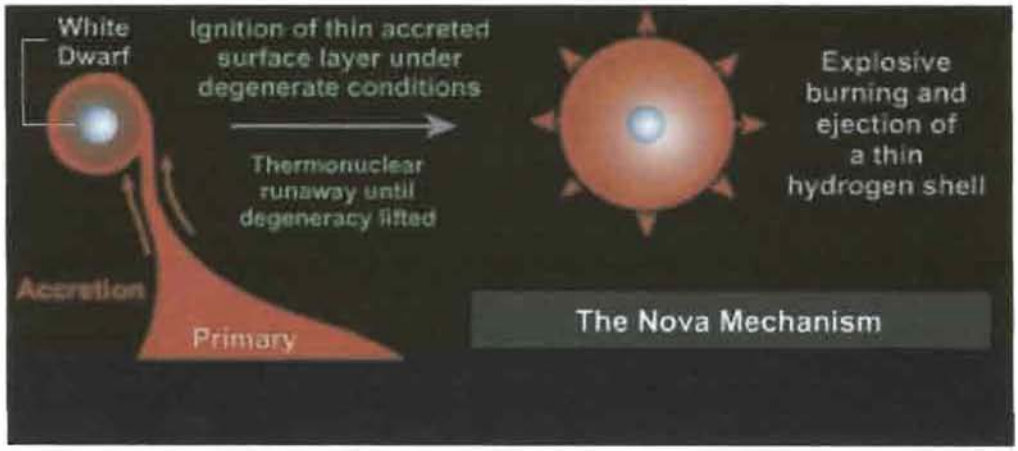

Figure 9: The mechanism by which a nova explodes.

Explosive burning also occurs during novae (**Figure 9**). This process begins when matter accretes onto a white dwarf from a more normal companion star. This accretion can be the result of either the companion star evolving to fill its Roche lobe (the gravitational equipotential surface enclosing

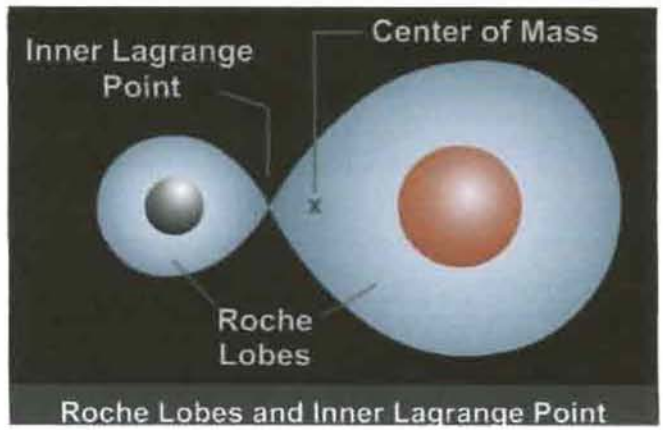

Figure 10: There is gravitational potential energy contour in a binary system that intersects itself in one point called the inner Lagrange point. The interior of this contour defines two regions, one around each star, called Roche lobes.

both stars, see **Figure 10**) and transferring matter via an accretion stream to the white dwarf, or a strong wind from the normal companion star that blows matter close enough to the white dwarf for it to be captured. The matter accretes through the Roche lobe onto the surface of the white dwarf. The accreted matter is a thin, highly dense, electron-degenerate envelope at the surface of the white dwarf [8]. Electron-degeneracy means all the electrons in the accreted material are in their lowest possible quantum state, which results from the high-pressure conditions [3]. The material of the white dwarf enriches this thin layer of accreted material. If the white dwarf is a CO-white dwarf, the accretion material is enriched by carbon and oxygen, and if it is an ONeMg-white dwarf, it is enriched by oxygen, neon, and magnesium.

Thermonuclear ignition begins after a "critical" mass has been accreted onto the white dwarf. This mass depends heavily on the mass of the white dwarf and the accretion rate [8]. These things determine the pressure at the bottom of the accreted material, where the ignition takes place.

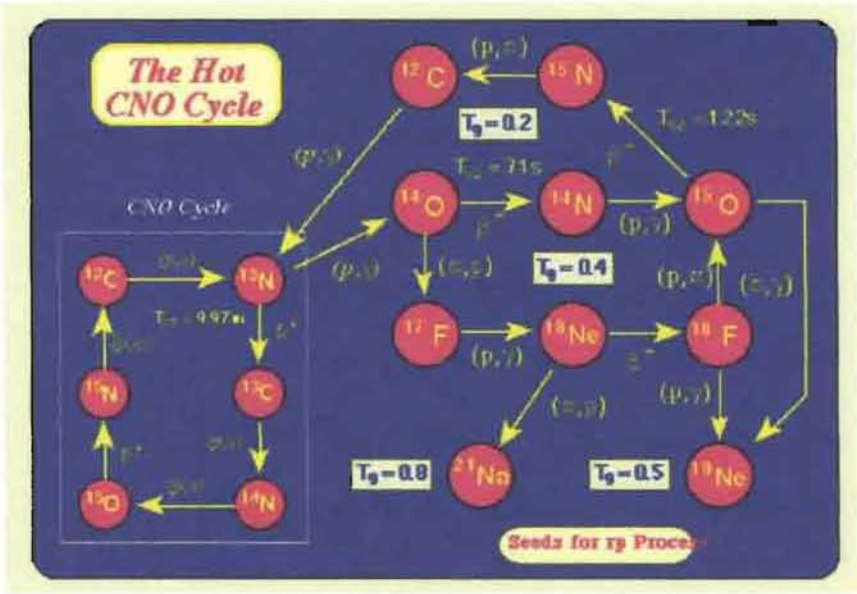

Figure 11: The hot CNO cycle begins when a temperature is reached that allows the $^{13}\mathrm{N}(\mathrm{p},\gamma)^{14}\mathrm{O}$ reaction begins to compete with the $\beta+$ decay. There are two parts of the cycle, occurring at different times, according to temperature.

Thermonuclear runaway is ignited via the pp-chain, resulting in a rapid increase in temperature at a constant pressure and density because of the degenerate conditions. As the temperature rises, the CNO and then hot CNO cycle is initiated (**Figure 11**), with high abundances of ^{12}C and ^{16}O until degeneracy is broken after the Fermi temperature has been attained [8].

The temperature rises rapidly at the bottom of the accreted material, causing a convective zone to develop. This convective zone quickly reaches the surface, allowing energy to be transported rapidly to the surface. Nuclei that are produced in the hot CNO cycle are also transported to the surface, more specifically those that can undergo beta+ decay (adding the release of beta+ decay energy to the energy being transported to the surface). This enormous luminosity thus causes a rapid expansion of the outer layers and the ejection of the outer shells. The energy released in this type of explosion ranges from 10^{46}-10^{47} ergs, with the hottest temperatures being around 0.2-0.3 GK.

Neutron stars can also accrete matter and explode in a similar fashion. These explosions are called X-ray bursts, having peak temperatures of 1-2 GK and releasing 10^{39}-10^{40} ergs of energy. Energy released here is lower because less hydrogen is accreted onto the neutron star before invoking a thermonuclear runaway. Because of the high temperatures, proton capture above the iron peak is possible. This process is called the rapid proton capture process, or rp-process.

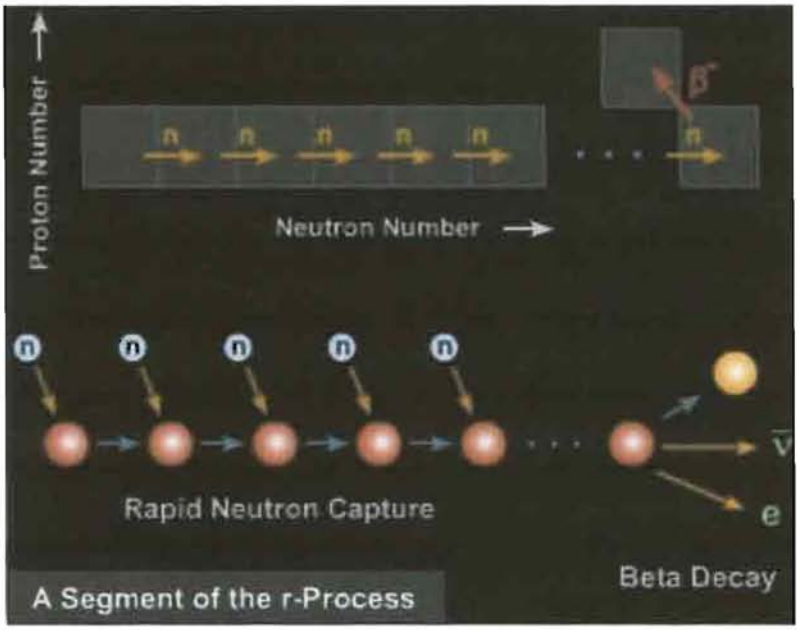

Figure 12: This is a part of the r-process.

There is also an explosive neutron capture process, called the rapid neutron capture process or r-process. This process requires much higher neutron concentrations than the s-process occurring during hydrostatic burning. This condition exists in during the compression of the matter in the core during core collapse or in the innermost region of the ejecta of a supernova. This material has undergone many electron and neutrino captures, so there are far more neutrons than protons. These extra neutrons provide the required neutron to heavy seed nucleus ratio. The r-process includes a large number of possible nuclei, so calculations are numerically taxing [5].

Current Thermonuclear Reaction Networks

3.1. Reaction Rates and Rate Equations

Nucleosynthesis and energy generation can be simulated for stellar burning processes with a large scale nuclear reaction network calculation that assumes a temperature and density time profile appropriate to a specific stellar scenario. The purpose of this simulation is to follow the time evolution of isotopic abundances and the reaction flux, which defines the reaction path for nucleosynthesis, and to calculate the

energy production as a function of time. The reaction network is generally composed of a system of first-order differential equations, with sink and source terms representing each of the possible nuclear reactions involved in the calculation.

An abundance, Y_i, of a nuclear species X_i (where X_i is defined as the mass fraction of this nuclear species) is given by

$$Y_i = \frac{X_i}{A_i} \tag{1.1}$$

where A_i is the atomic weight of the nucleus i. The mass fraction, which is the fraction of nucleons in the sample which are tied up in the form of particles of species i, is defined by

$$\begin{aligned} X_i &\equiv \frac{n_i A_i}{\rho N_A} \\ \sum_i X_i &= 1 \end{aligned} \tag{1.2}$$

where n_i is the number density (the number of species i per unit volume), ρ is the mass density, and N_A is Avogadro's number [1].

The nuclear network is defined by a set of differential equations detailing the time evolution of these abundances. These are expressed in terms of the time derivative of the abundance of each isotope and the reaction rates of the possible production and depletion reactions [8]:

$$\begin{aligned} \frac{dYi}{dt} &= \sum_j N_j^i \lambda_j Y_j + \sum_{j,k} N_{j,k}^i \rho N_A < j,k > Y_j Y_k \\ &+ \sum_{j,k,l} N_{j,k,l}^i \rho^2 N_A^2 < j,k,l > Y_j Y_k Y_l . \end{aligned} \tag{1.3}$$

In this equation, N_A stands for Avogadro's number. The term $\langle j,k \rangle$ represents the integrated cross-sections of particles *j* and *k*, which will be explained shortly. The three terms on the right side of the equation stand for three types of reactions. The first term is categorized as decay and photodisintegration processes, which are proportional to a decay constant λ_j. The second term represents two particle capture processes, which are proportional to $\rho N_A < j,k >$. The third term represents three particle interactions, which are proportional to $\rho^2 N_A^2 < j,k,l >$. The reaction rate of each nuclei in a two or three particle reaction depends on the mass density, ρ. The N^i's are given by $N_j^i = N_i$, $N_{j,k}^i = N_i/(N_j!N_k!)$, and $N_{j,k,l}^i = N_i/(N_j!N_k!N_k!)$ [8]. Each of these N^i's stands for a positive or negative number specifying how many particles of species *i* are created or destroyed in the reaction taking place. When two or three identical particles interact with each other, the denominators of these N^i's prevent double counting.

The reaction flux, mentioned above, can be described by the equation [8]

$$F_{i,j} = \int \left[\frac{dY_i}{dt}_{(i \to j)} - \frac{dY_j}{dt}_{(j \to i)} \right] dt . \tag{1.4}$$

$F_{i,j}$ is the time integrated net reaction flow between two isotopes *i* and *j*, and defines the main reaction path(s) along which nucleosynthesis will take place. The amount of energy produced during nucleosynthesis can be determined from the flux and the Q-values, $Q_{i,j}$, of the reactions taking place. The Q-value is the amount of energy released or used in a thermonuclear reaction. The energy, ε, is calculated from [8]

$$\varepsilon = \sum_{i,j} F_{i,j} Q_{i,j} . \tag{1.5}$$

All of the equations above depend critically on the thermonuclear rates for reactions that have occurred during the nucleosynthesis process. These rates must be known accurately, either through experiment or theory, to accurately determine the time evolution of the isotopic abundances, energy, and flux.

There are different types of thermonuclear reaction rates for each of the different types of reactions. First, we will look at beta-decays. The decay rates of β-unstable particles, labeled λ_j, are usually determined from experimental lifetimes τ_i or from the half lives $T_{1/2}^i$ through the relations [8]:

$$\lambda_i = \frac{1}{\tau_i} = \frac{\ln 2}{T_{1/2}^i}. \tag{1.6}$$

If the experimental half-life is not known, the decay rate can be calculated in terms of the β-strength function. See [8] for more details.

For interactions between two particles j,k, the most basic piece of information is the nuclear cross section, σ. The cross section is the probability per pair of particles for occurrence of a reaction [2,5]:

$$\sigma = \frac{\text{number of reactions/target s/unit time}}{\text{flux of incoming projectiles/unit time}} = \frac{r/n_j}{n_k v} \tag{1.7}$$

where n_j is the number density of the target nuclei and n_k is the number density of the projectiles. The above equation is true only when the relative velocity between the targets with the number densities n_j and n_k is constant, having the value v. When this equation holds, r can then be expressed as

$$r = \sigma v n_j n_k. \tag{1.8}$$

In general, the targets and projectiles have distributions of velocities, so then r becomes [5]

$$r_{j,k} = \int \sigma\left(\left|v_j - v_k\right|\right)\left|v_j - v_k\right| d^3 n_j d^3 n_k \,. \tag{1.9}$$

This integral can be evaluated for different types of particles and the distributions that characterize them. For astrophysical situations Maxwell-Boltzmann statistics often apply. This means the integral can be solved with [5]

$$d^3 n = n\left(\frac{m}{2\pi k_B T}\right)^{3/2} \exp\left(-\frac{mv^2}{2k_B T}\right) d^3 v \,. \tag{1.10}$$

Thus, n_j and n_k can be moved outside the integral in equation (1.8), and the number of reactions per cm^3 per second can be expressed as $r_{j,k} = \langle \sigma v \rangle_{j,k} n_j n_k$, where $\langle \sigma v \rangle$ stands for the velocity integrated cross-section. The mean lifetime for a particle j against an interaction with particle k can be expressed as

$$\tau_k(j) = \frac{1}{\langle \sigma v \rangle_{j,k} n_k} \,. \tag{1.11}$$

For this interaction between these two particles, we can now express the stellar reaction rate $\langle j,k \rangle$ in terms of the cross section, the reduced mass μ, the particle energy E (center of mass energy), and the temperature T [5,8]:

$$\langle j,k \rangle \equiv \langle \sigma v \rangle_{j,k} = \left(\frac{8}{\mu\pi}\right)^{1/2} (k_B T)^{-3/2} \int_0^\infty E\sigma(E) \exp\left(-\frac{E}{k_B T}\right) dE \,. \tag{1.12}$$

All of the equations used above treated each particle as a bare nucleus. In reality, in astrophysical plasmas this is not completely true. To account for the other particles present (other nuclei and electrons), and the resulting change in Coulomb repulsion at high densities and/or low temperatures, a screening factor must be introduced. For a

short introduction, see [5]. For a further discussion of three particle interactions, electron captures, neutrino captures, or photodisintegrations, see [10,11].

3.2. Solving the Nuclear Network

There are many methods that can be used to solve a set of first-order differential equations, but the character of the nuclear reaction network limits which of these methods can be used because the network typically contains a wide range of rates. Such equations are known as stiff, meaning that there is a wide range of timescales in the problem and they are numerically unstable unless particular care is taken in their integration. Thus, a system is stiff when the limitation of timestep size is due to numerical stability rather than accuracy [5]. The integration of the rate equations (the differential equations outlined above) must be broken up into short intervals in order to update the hydrodynamics variables. These abundances are tracked in a grid-based system, including hundreds to thousands of these cells for a one-dimensional calculation, and millions for the coming generation of fully three-dimensional models. Because of memory storage concerns, low-order methods are favored since they do not require the storage of as much data from prior steps. The higher order methods do not necessarily create a more accurate calculation in these simulations since errors in the fluid dynamics and reaction rates are on the order of a few percent or more [5].

The stiffness of these equations can be demonstrated with a simple example: the PP chain. The first and second reactions of the PP chain have very different timescales. The first reaction, $^{1}\mathrm{H}(p,e^{+}\nu)^{2}\mathrm{H}$, is a weak reaction, requiring the conversion of a proton into a neutron, releasing a positron and a neutrino. The reaction timescale in this case is

on the order of billions of years for solar conditions. However, the second reaction in the chain, $^2\mathrm{H}(p,\gamma)^3\mathrm{He}$, occurs on a timescale of a few seconds in conditions similar to the solar interior. The rates of these reactions, two of the most basic reactions that occur in stars with mass equal to or less than solar mass, differ by 17 orders of magnitude. Many other nucleosynthesis reactions are similarly this stiff, making for the solving of the reaction equations extremely difficult with the most sophisticated methods [5].

To solve for a set of nuclear abundances, the time derivative can be calculated using [5]

$$\frac{\boldsymbol{Y}(t+\Delta t)-\boldsymbol{Y}(t)}{\Delta t} = (1-\Theta)\dot{\boldsymbol{Y}}(t+\Delta t)+\Theta\dot{\boldsymbol{Y}}(t). \tag{1.13}$$

If $\Theta = 1$, the above equation become the explicit Euler method. For $\Theta = 0$, it is the implicit backward Euler method. Both of these methods are first order accurate. For $\Theta = 1/2$, equation (12) is the semi-implicit trapezoidal method, which is second order accurate. The implicit treatment is the most successful for most nuclear networks because it is so stable [5]. For the $\Theta = 0$ or fully implicit case, equation (1.12) becomes

$$L(t+\Delta t) \equiv \frac{\boldsymbol{Y}(t+\Delta t)-\boldsymbol{Y}(t)}{\Delta t} - \dot{\boldsymbol{Y}}(t+\Delta t) = 0. \tag{1.14}$$

Now, this equation can be solved with a root finding method. This is done most often using the Newton-Raphson method [12]. This method is based on doing the Taylor series expansion of $L(t+\Delta t)$, with a trial change in abundances [5]

$$\Delta \boldsymbol{Y} = \left(\frac{\partial L(t+\Delta t)}{\partial \boldsymbol{Y}(t+\Delta t)}\right)^{-1} L \tag{1.15}$$

where $\partial L / \partial \boldsymbol{Y}$ is the Jacobian of L. Iteration should continue until $\boldsymbol{Y}(t+\Delta t)$ converges. There are potential problems with singularities in the Jacobian. The matrix elements of the Jacobian have the form [5]

$$\frac{\partial L_i}{dY_j} = \frac{\delta_{i,j}}{\Delta t} - \frac{\partial \dot{Y}_i}{\partial Y_j} = \frac{\delta_{i,j}}{\Delta t} - \sum \frac{1}{\tau_j(i)}. \tag{1.16}$$

The symbol $\delta_{i,j}$ is the Kronecker delta, and $\tau_j(i)$ is the destruction timescale of nucleus i with respect to nucleus j for each reaction. The sum over all possible timescales for nucleus i, the second term in equation (1.15), indicates that more than one reaction is possible for a particular nucleus. This term is dominated by the fastest reactions, meaning those having the shortest destruction timescales. The diagonal elements of the matrix have two competing terms, since $i = j$: the timestep and the destruction timescale of nucleus i. With a problem near equilibrium, the destruction and the corresponding production rates are very fast when compared to the most optimal timestep size. Thus, the timestep term Δt ends up being neglected, leading to numerically singular matrices. Scaling the equilibrium timescales by a factor that brings them closer to the preferred timestep term can skirt this issue. This has been done, but there are currently other more promising approaches being looked into as well. For more information, please see [5].

The Stochastic Algorithm for Element Production

4.1. Formulation of the Problem

This section will now demonstrate how the nucleosynthesis problem outlined in the preceding sections can be simulated stochastically. The main idea of this algorithm is to push a test particle along a reaction path guided by its probabilities for each possible

thermonuclear transition. Each of these test particles will go on a "random walk" through the chart of the nuclides, in the n and z plane. This is effectively a numerical path integral. This statistical formulation of the problem takes full advantage of the intrinsically random nature of particle collisions in an astrophysical plasma.

In principle, all isotopes in a nuclear reaction network can be coupled by various nuclear reactions. In practice, any given isotope is typically only connected to a few other isotopes by strong reactions. This means that the matrices that appear in the Newton-Raphson iteration are sparse (the non-zero entries are few in number). The stochastic method takes natural advantage of the sparse nature of the element production network: because the test particles sample the reaction paths statistically, they follow only those reaction links from isotope to isotope that have significant rates. Thus, no computational time is wasted on transitions that are extremely unlikely to occur.

As a consequence, the stochastic method has extremely benign scaling behavior as the network size is increased, with the time to compute generally increasing more weakly than linearly with the number of isotopes in the network. Although in principle standard methods could also take advantage of the sparseness of the matrices, in practice not much has been done to do so in commonly used codes. As a consequence, standard methods have poor scaling behavior as network size is increased, with the time required for computation often scaling quadratically or worse with the number of isotopes in the network.

We begin the simulation by choosing a total number seed nuclei, or test particles, $N = \sum_i N_i$. We then choose a test volume, V, in which the mass density is ρ. The stellar scenario that we are simulating determines this mass density and temperature. The

initial population, as above, is described by the abundance of each seed nucleus, Y_i. Each nuclear species has N_i test particles in V to represent this abundance. Using the information on reaction rates from section *3.1* above, we know that the abundance is $Y_i = {}^{X_i}\!/_{A_i}$, but we can also expand this as

$$Y_i = \frac{X_i}{A_i} = \frac{n_i}{\rho N_A} = \frac{N_i}{\rho V N_A} \tag{1.1}$$

where n_i is the particle number density of nucleus i and N_A is Avogadro's number. This results from $N_i = n_i V$; the total number of each nucleus i is the number density of that nucleus multiplied by the total volume. Since we assume that we know the initial abundances Y_i, we can rearrange equation (1) and write

$$N_i = V \rho N_A Y_i . \tag{1.2}$$

Since we know that the total number of test particles is $N = \sum_i N_i$, we can substitute this into equation (2) to get

$$N = \sum_i N_i = V \rho N_A \sum_i Y_i . \tag{1.3}$$

This can be rearranged to find the total initial volume for the calculation:

$$V = \frac{N}{\rho N_A \sum_i Y_i} . \tag{1.4}$$

Thus, the total number of seed nuclei of species i is $N_i = fY_i$, where $f = {}^{N}\!/_{\sum_i Y_i}$, which is completely independent of volume and mass density. The total number of nucleons, n_T is the total number of protons and neutrons in the system,

$$n_T = \sum_i N_i A_i \ .(1.5)$$

Since all reactions conserve nucleon number, n_T is a conserved quantity [4].

4.2. Moving Test Particles with Probabilities

Now that we know how to count each species involved in the calculation, we must define how the particle populations will change with time. Each nucleus will still be described as having a certain number of possible reactions to undergo, only now, instead of solving the reaction equations involving that particular particle implicitly, the probabilities for the different reactions to occur will be calculated explicitly by stochastic means. As above, we are trying to solve the equation

$$\frac{dY_i}{dt} = \sum_j N_j^i \lambda_j Y_j + \sum_{j,k} N_{j,k}^i \rho N_A < j,k > Y_j Y_k + \sum_{j,k,l} N_{j,k,l}^i \rho^2 N_A^2 < j,k,l > Y_j Y_k Y_l \ . \quad (2.1)$$

Again, the first term relates to the β -decays or photodisintegrations, the second term characterizes the two-body interactions, and the last term the three-body interactions. In the stochastic algorithm, we "move" with the particle to each position in the nz plane. Thus, when we are sitting in a specific spot in the plane, we only take into consideration the depletion of the current isotope that our test particle occupies. Consider equation (2.1) for one particle, i, which has the possibility of a beta decay and a two body reaction with a particle k. We may write out the one and two body interaction terms as (including only the depletion terms)

$$\frac{dY_i}{dt} = \lambda_i Y_i + \rho N_A < i,k > Y_i Y_k \quad (2.2)$$

This equation may now be written with a finite timestep as

$$\Delta Y_i = \left(\lambda_i Y_i + \rho N_A < i,k > Y_i Y_k\right)\Delta t \,. \tag{2.3}$$

We can now express the change in abundance as a probability by dividing through by the abundance, Y_i:

$$\frac{\Delta Y_i}{Y_i} = \left(\frac{\lambda_i Y_i}{Y_i} + \frac{\rho N_A < i,k > Y_i Y_k}{Y_i}\right)\Delta t = \left(\lambda_i + \rho N_A < i,k > Y_k\right)\Delta t \,. \tag{2.4}$$

So,

$$\begin{aligned} \frac{\Delta Y_i}{Y_i} &= P_{i\to j} + P_{i+k} \\ P_{i\to j} &= \lambda_i \Delta t \\ P_{i+k} &= \rho N_A < i,k > Y_k \Delta t \end{aligned} \tag{2.5}$$

where P's in equation (2.5) represent the probability for the depletion of particle i. As a result, the probability for nothing to occur is $P_0 = 1 - P_{i\to j} - P_{i+j}$ (as long as these are the only two possible reactions for this nucleus, as we are assuming in this illustrative example). One can recognize easily that these probabilities are essentially the same thermonuclear reaction rates used in the previously explained method multiplied by a timestep. The parameter P_0 determines the length of the timestep (see below). Since the probabilities are normalized, it obviously must lie in the interval 0 to 1. Smaller values of P_0 give larger timesteps and therefore faster calculations, but less accuracy for the low abundance of isotopes. For the calculations presented here, we have found $P_0 = 0.99$ to be a good tradeoff of accuracy versus time. Therefore, for all results presented in this paper, this value of P_0 has been used.

The timestep, Δt, is calculated using this set value of P_0. This in effect renormalizes the other calculated probabilities to the scale of 0.99-1.0, as opposed to the normal scale of probabilities of 0-1. The timestep is calculated using the equation

$$\Delta t = \frac{1 - P_0}{\sum_n r_n}. \tag{2.6}$$

This timestep must be chosen relative to the reaction timescales of each nucleus' possible thermonuclear reactions. Do not get this timestep confused with the (generally much larger) time intervals used for plotting. It seems optimal to split the total simulation time into no more than 50 plotting time intervals. At the end of each time interval, the abundances of all species are recorded, and a new plotting time interval is begun. Inside of these plotting time intervals, the particles are pushed over their individual timesteps, Δt.

The reaction rates that we calculated were from the Thielemann nuclear reaction library (http://ie.lbl.gov/astro/friedel.html). This library includes all of the possible rates described by the reaction rate equations above. This library contains parameters for each possible reaction to use in the calculation of a reaction rate. For the one-body reactions, the rate calculated from the library is essentially constant, and does not need information about the mass density, temperature, or abundances of surrounding nuclei. The reaction library gives one value for each of these one-body reactions, and the rate is calculated as $\exp(R)$, where R is the value from the reaction library.

For the two-body reactions, the rate calculated from the library only includes the factors $N_A < i, j >$. For each possible two-body reaction, a set of seven parameters is given. The rate is then calculated with the following formula

$$\mathrm{R}=\exp\left[a_1+\frac{a_2}{t9}+\frac{a_3}{(t9)^{1/3}}+a_4\ t9^{1/3}+a_5\ t9+a_6\ t9^{5/3}+a_7\ \ln(t9) \right] \tag{2.7}$$

Now that we have all the pieces in place to calculate the probability of every possible nucleus in the simulation, we are ready to summarize the steps that are actually taken in the algorithm. They are as follows:

1. Input initial abundances, temperature, density, start and end times of entire simulation, and total number of initial seed nuclei (test particles).
2. Read and calculate all thermonuclear rates included in simulation and calculate total initial nucleon number. (Since this quantity is conserved, its constancy in the calculation can serve as a numerical consistency check)
3. Divide the total simulation time into plotting time intervals logarithmically.
4. During first time interval, for every single test particle of every type of nucleus, calculate the nucleus-specific timestep to take. Next, calculate the probabilities for all possible reactions available to that nucleus. "Throw the dice," meaning, generate a random number. If this number is less than 0.99, nothing occurs, and the particle does not move during this timestep. If the random number is between 0.99 and $0.99 + P_1$, the reaction 1 occurs and the test particle is moved to the resulting nucleus from its initial position. Likewise, if the random number falls between $0.99 + P_1$ and $0.99 + P_1 + P_2$, reaction 2 occurs. This logic is used for all probabilities that have been calculated for this test particle (the sum of all probabilities, $P_0 + P_1 + P_2 + ... + P_n$ is 1).
5. Whether or not the particle has been moved, a new timestep is now calculated, then another set of probabilities are calculated for the next trial random

number. Repeat these steps for all test particles (meaning all species as well) until the end of the plotting time interval is reached.

6. Record the populations of the test particles at this point then repeat steps 4 and 5 for all consequent plotting timesteps.

After all these steps are completed, an output file is generated containing the information for the evolution of isotopic abundances over time.

As one can see, the inherent stability of this algorithm is based in the integer arithmetic that is used to perform the most important parts of the calculation. Unlike the implicit Euler method of solving the rate equations, this algorithm takes full advantage of the sparseness of the matrices. This simulation must only calculate the numerical path integral of the species with which a test particle is or becomes associated. Thus, a less-than linear speedup is expected when the network used for our test applications is enlarged. The only additional calculations for an enlargement of the network to involve more massive isotopes would be to calculate more rates from the Thielemann library once, at the beginning of the program. Generally, one needs to also increase the number of test particles to maintain the accuracy if more species are populated.

Since the stochastic algorithm uses integer addition and subtraction for the counting and moving of test particles, the results with lower mass fractions have discrete statistical fluctuations that are not characteristic of the ordinary differential equation solver results. As a consequence, the stochastic results fluctuate around the solutions to the implicit method. If the stochastic results are averaged over a few data points, the results match those of the implicit method rather well. Since these fluctuations are statistical in nature, the stochastic abundances should converge to the solutions from the

implicit solver with an error given by the square root of the number of counts for an isotope.

In the present calculations, there may be some fluctuations present in addition to the expected statistical ones that are associated with the approximate method currently in use to stop the calculation at fixed time intervals for plotting purposes. Since the calculation is stochastic, forcing it to stop at a fixed time (for convenience in plotting for comparison with standard methods) is not natural. In the current approximate scheme, if the projected timestep of a test particle is calculated to be longer than the time to the next plot interval, the nucleus is simply left in its current state. Since there is a small probability that the (short) omitted time interval would have produced a transition, this artificially moves a few test particles between time bins and can contribute fluctuations in addition to the statistical ones. This appears to be a minor problem, and will be corrected in future work. Preliminary tests of a more correct algorithm for terminating the timestep indicate a reduction in fluctuations over that with the current method.

Testing of the Algorithm

5.1. The CNO cycle

For the first test of the stochastic algorithm, we chose to use the CNO cycle, described in the hydrostatic burning section above. This cycle is well known, and many results have been obtained that are found in textbooks and papers. For this calculation, only the reaction rates from the carbon isotopes to the sodium isotopes were included (for instance, there were no proton-proton reactions allowed). Constant temperature and density were also used, which is not completely uncharacteristic of a hydrostatic burning

process. This simplification also enables us to concentrate on the properties of the algorithm more easily than in a more reliable calculation with a temperature and density profile.

The CNO calculation results for the backwards Euler implicit method are shown in **Figure 13**. The results from our stochastic algorithm are shown in **Figure 14**.

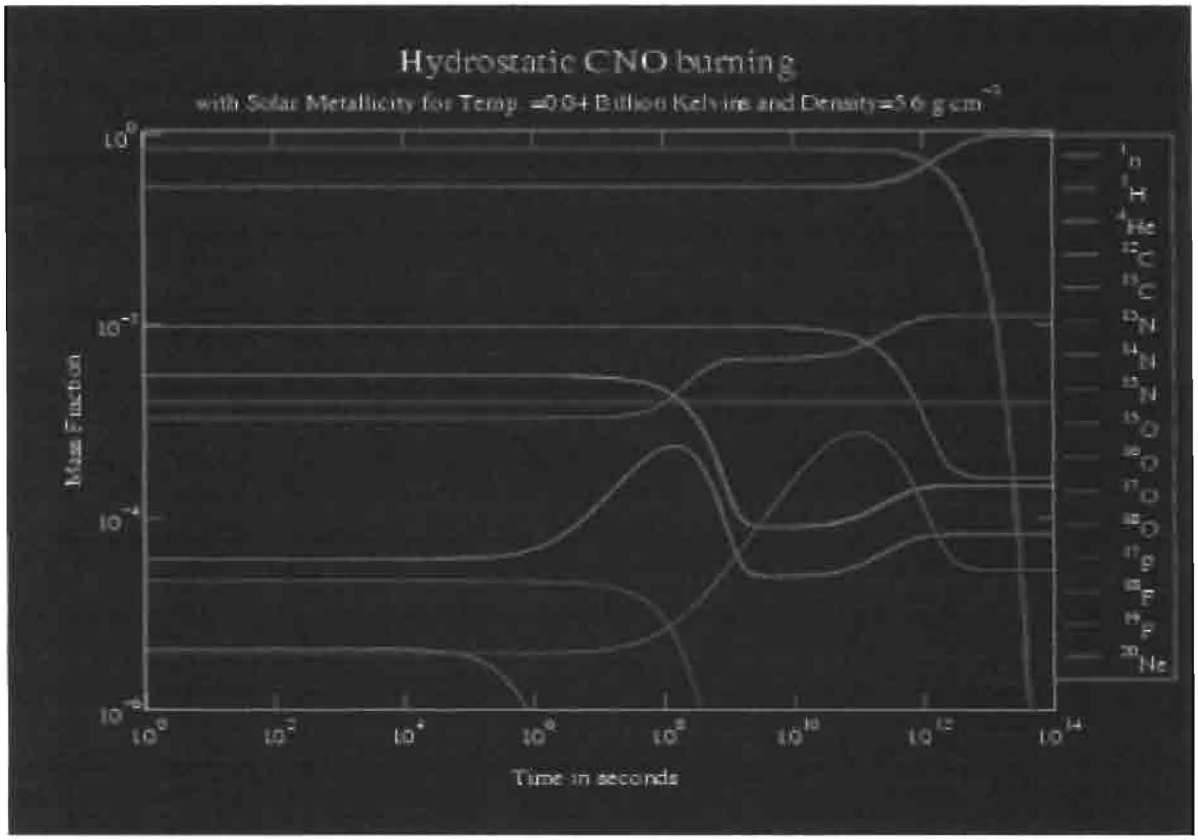

Figure 13: The accepted results for the CNO cycle, using the implicit method of solving.

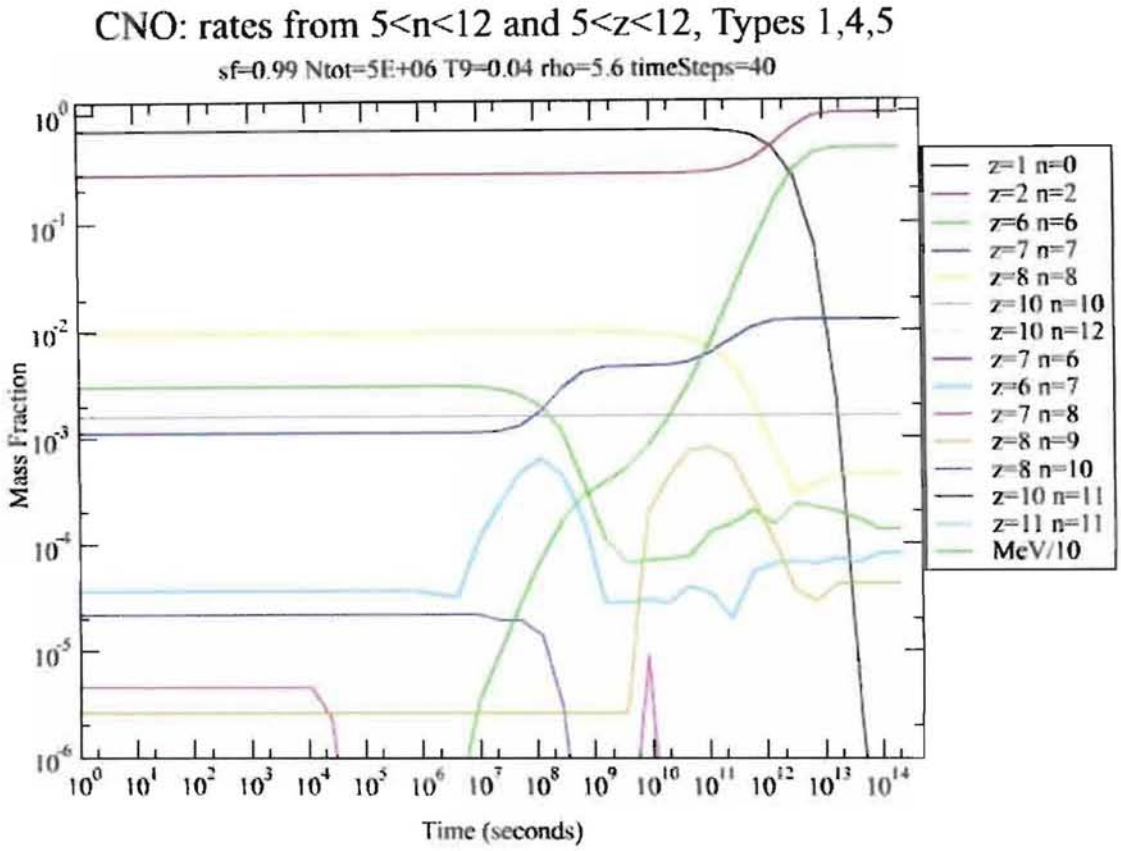

Figure 14: Results from the stochastic method. Notice the very good agreement down to mass fraction of about 10^{-4} and a reasonable agreement down to a mass fraction of 10^{-6}. The rates included in the program are noted in the title of the plot. Types 1, 4, and 5 limit the calculation to one-body decays and charged particle capture reactions.

The results are very similar, even quantitatively. One sees, however, the fluctuations at low mass fraction. Adding more test particles to the simulation can lessen this fluctuation, but doing so increases the computational time linearly.

5.2. The Hot CNO Cycle

The second test of this algorithm was done with the hot CNO cycle in an ONeMg white dwarf nova. This test was also done with constant temperature and density conditions. Although not completely realistic, this lessens the number of variables in the calculation and facilitates simple comparisons. This calculation was also done with the implicit backwards Euler method, shown with the stochastic results in the plot below, **Figure 15**.

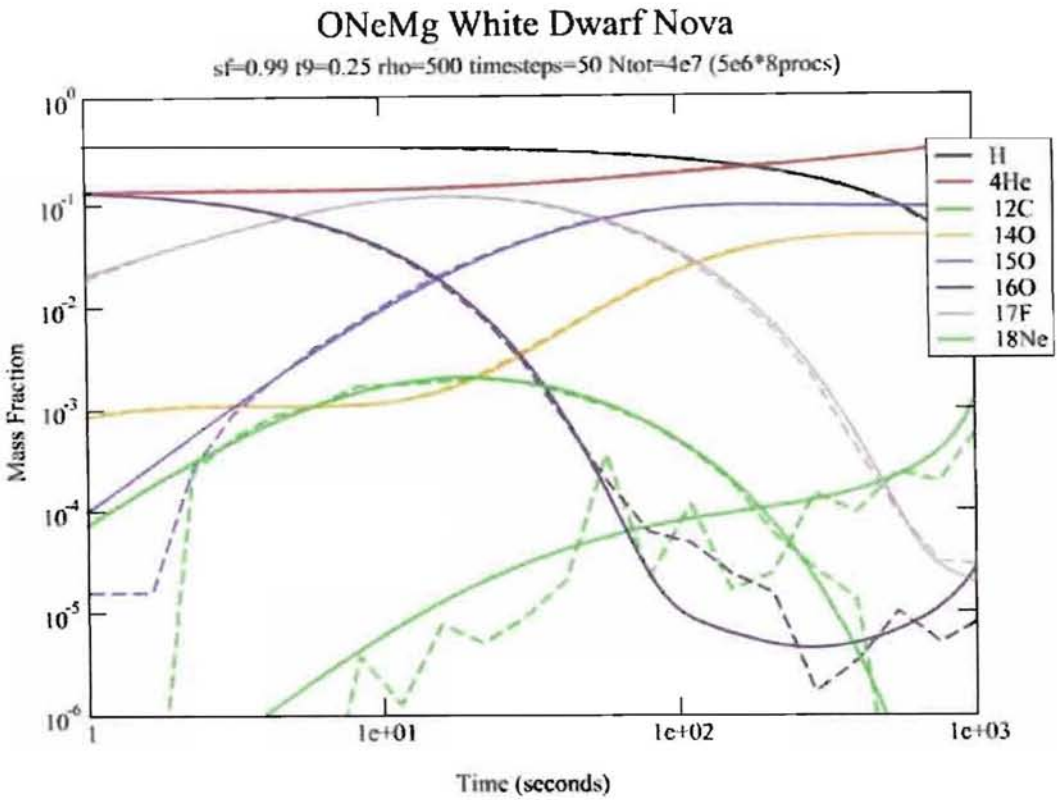

Figure 15: This plot compares the results from the implicit and stochastic methods. The dashed lines are the stochastic results, while the solid lines are the implicit results.

Both test cases demonstrate that the stochastic algorithm is a feasible method of solving this stiff system of differential equations. One sees the fluctuations again, in the low mass fraction region of the plot. Although there is some uncertainly and fluctuation around the lower mass fractions, they clearly reproduce an average of the results found using the implicit method.

5.3. Parallelizing this Algorithm

The stochastic algorithm was also implemented on GEAT (General Engine for Astrophysics at Tennessee), an 8-node Beowulf cluster. Since this algorithm mainly

involves "throwing dice" or picking random numbers, identical simulations (with different random number seeds) can be run on each of the 8 processors with no communication until the end of the simulation. This effectively means that you can run a calculation 8 times larger (8 times more test particles, making the calculation more accurate) in almost the same amount of time that you could run one calculation. The scaled speedup of the system for the hot CNO cycle tests was 7.8/8 = 98% (see **Figure 17**) for the largest calculation.

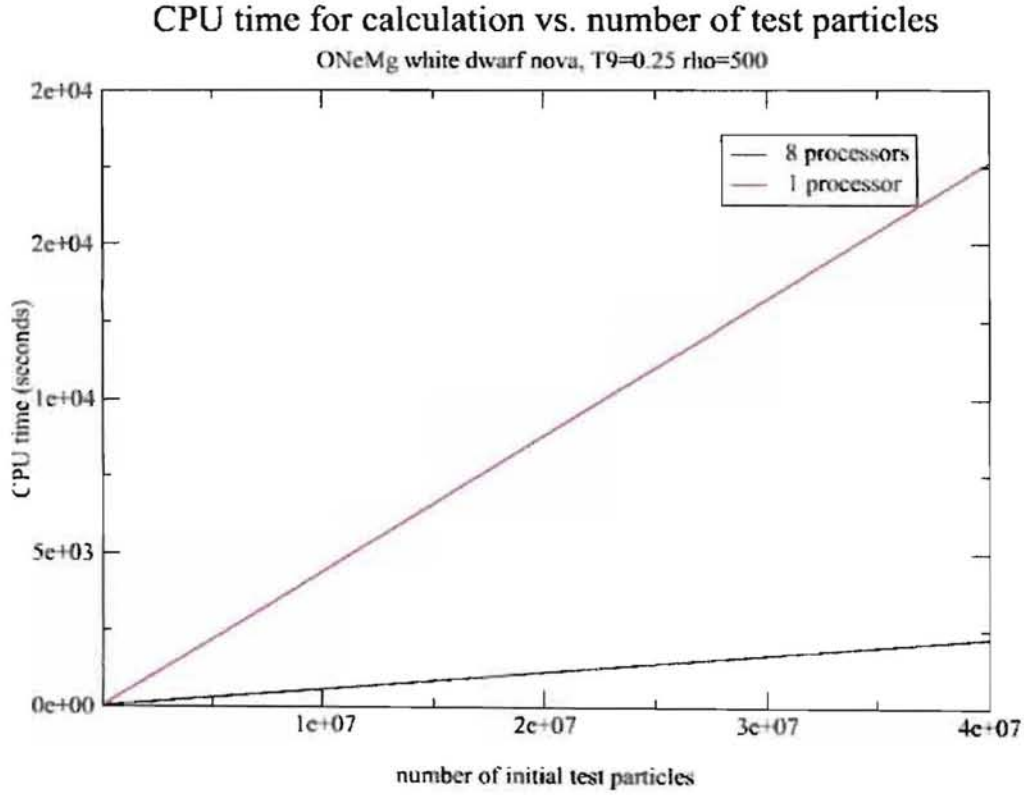

Figure 16

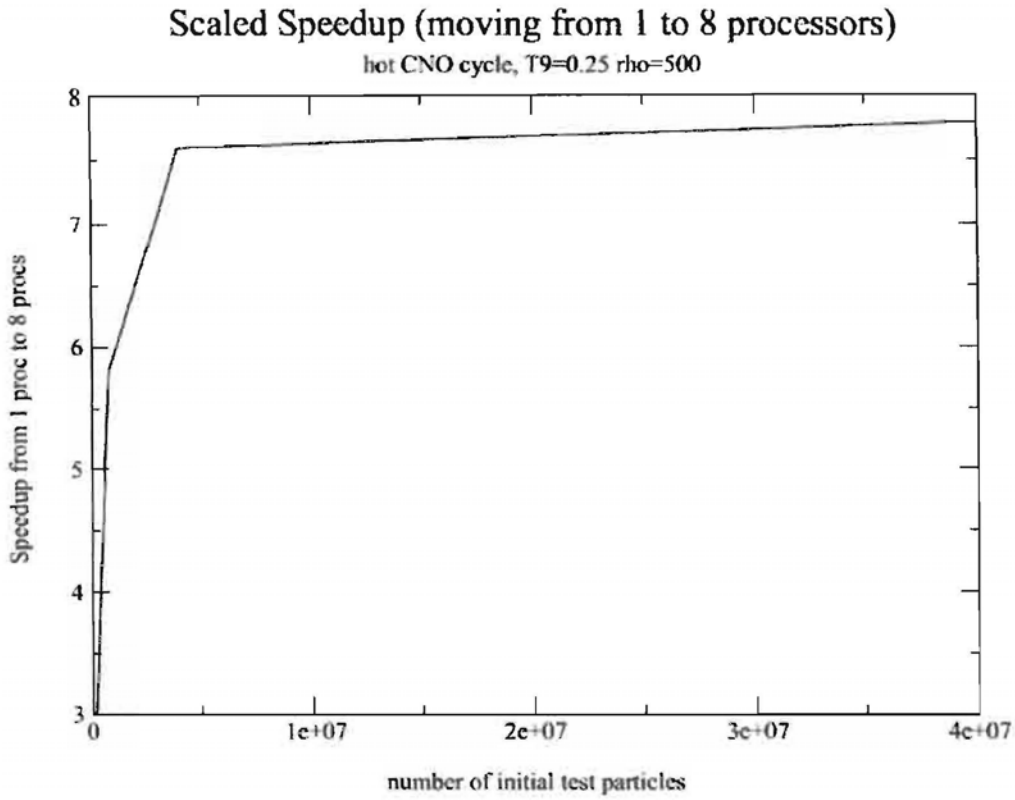

Figure 17

The results from each node may be collected by the main node, using MPI (Message Passing Interface). Since the results first are expressed in integer numbers of test particles occupying the resulting isotopes, these numbers that were split up at the beginning of the calculation to each processor are just added together again at the end.

You must, however, be careful to choose different random number seeds on each of the processors. Because the "random number" generator is actually pseudorandom (see below), choosing the same random number seed for each processor would produce identical results. Currently, the random number generator being used is the ran3 function from [12], changing only the real variables to 8-bit precision. This is a pseudorandom generator—this means that the numbers produced by the generator have a definite

pattern. For this algorithm, it is extremely beneficial to look for a pseudorandom number generator exhibiting "random" behavior and having a long period. Most good pseudorandom number generators have a period of about 2^{31}. Currently, I have different seeds for each processor hardwired into the program. I am currently looking at more efficient and more "random" ways of generating random numbers on a parallel system.

Conclusion

In this paper, I have concentrated on showing that our new stochastic algorithm for element production produces acceptable results for two test cases. At mass fractions above about 10^{-4} the results are almost a perfect match to the implicit method using the same rate library. Although this method might not be as accurate at lower mass fractions as the implicit method, it provides a rough estimation of the abundances at this level that can be averaged to a similar result. The initial indications are that this algorithm is extremely fast related to standard ones, particularly for very large networks.

In addition, I have shown that a parallel version gives almost 100% speedup on an 8-node Beowulf cluster. This is expected, since the stochastic nature implies inherent parallelism. While it is true that the present work indicates that this algorithm seems to be a viable solution for modeling the evolution of isotopic abundances over time, there is still much work to be done. We would like to concentrate on these topics in the near future: working out a better method for making plotting time intervals, generate better random numbers in a parallel environment, and coupling this method with a hydrodynamics code to make highly realistic simulations of element production in stellar explosions.

References

[1] W.D. Arnett, *Supernovae and Nucleosynthesis*, Princeton: Princeton Univ., 1996.

[2] D. Clayton, *Principles of Stellar Evolution and Nucleosynthesis*. Chicago: University of Chicago Press,1983.

[3] M. Guidry, Neutrino Transport and Large-Scale convection in Core-Collapse Supernovae, In *Cambridge Contemporary Astrophysics: Nuclear and Particle Astrophysics, proceedings of the Mexican School on Nuclear Astrophysics, held in Guanajuato, Mexico, August 13-20, 1997.* (ed. J. G. Hirsch and D. Page) p. 115-51. Cambridge University Press, 1998.

[4] M. Guidry, private communications and unpublished notes, 2001-2002.

[5] W.R. Hix & F.K. Thielemann, Journal of Computational and Applied Mathematics, **109**, 321-351, 1999.

[6] S. Starrfield, Thermonuclear Processes and the Classical Nova Outburst, In *Classical Novae* (ed. M. F. Bode and A. Evans) p. 39. New York, John Wiley & Sons Ltd, 1989.

[7] F.-K. Thielemann, F. Brachwitz, C. Freiburghaus, S. Rosswog, K. Nomoto, K. Iwamoto, K. Langanke, G. Martininez-Pinedo, D.J. Dean, W.R. Hix, M.S. Strayer, Abundances from Supernovae, In *Supernovae and gamma-ray bursts: the greatest explosions since the Big Bang. Proceedings of the Space Telescope Science Institute Symposium, held in Baltimore, MD, USA, May 3 - 6, 1999*, (ed. Mario Livio, Nino Panagia, Kailash Sahu) p. 258-286. Space Telescope Science Institute symposium series, Vol. 13. Cambridge, UK: Cambridge University Press, 2001.

[8] M. Wiescher, Signatures of Nucleosynthesis in Explosive Stellar Processes, In *Cambridge Contemporary Astrophysics: Nuclear and Particle Astrophysics, proceedings of the Mexican School on Nuclear Astrophysics, held in Guanajuato, Mexico, August 13-20, 1997.* (ed. J. G. Hirsch and D. Page) p. 79-114. Cambridge University Press, 1998.

[9] Pictures taken from http://www.onlineastronomy.com, accessed April 2002.

[10] W.A. Fowler, G.E. Caughlan, B.A. Zimmerman, 1967 *Ann. Rev. Astron. Astrophys.* **5**, 525.

[11] W.A. Fowler, G.E. Caughlan, B.A. Zimmerman, 1975 *Ann. Rev. Astron. Astrophys.* **13**, 69.

[12] W.H. Press, S.A. Teukolsky, W.T. Vetterling, B.P. Flannery, *Numerical Recipes, 2nd ed.* Cambridge: Cambridge Univ., 1992.